Applied Physics Letters

Manipulating transverse photovoltage across plasmonic triangle holes of symmetry breaking

Cite as: Appl. Phys. Lett. **114**, 171102 (2019); https://doi.org/10.1063/1.5093894
Submitted: 25 February 2019 . Accepted: 22 April 2019 . Published Online: 01 May 2019

Marjan Akbari, Jie Gao, and Xiaodong Yang

Applied Physics Letters ARTICLE scitation.org/journal/apl

Manipulating transverse photovoltage across plasmonic triangle holes of symmetry breaking

Cite as: Appl. Phys. Lett. **114**, 171102 (2019); doi: 10.1063/1.5093894
Submitted: 25 February 2019 · Accepted: 22 April 2019 ·
Published Online: 1 May 2019

Marjan Akbari, Jie Gao,[a] and Xiaodong Yang[a]

AFFILIATIONS

Department of Mechanical and Aerospace Engineering, Missouri University of Science and Technology, Rolla, Missouri 65409, USA

[a]Electronic addresses: gaojie@mst.edu and yangxia@mst.edu

ABSTRACT

The transverse photo-induced voltages generated by the photon drag effect under normally and obliquely incident circularly polarized light across the plasmonic symmetry-breaking isosceles-triangle holes and right-triangle holes have been characterized. It is observed that the sign of transverse photovoltage flips when the incident circular polarization is switched for both types of plasmonic triangle holes. However, the unbalanced photovoltage between two circular polarizations is achieved across the plasmonic right-triangle holes, compared to the balanced photovoltage in the plasmonic isosceles-triangle holes. Such manipulation of the sign and the amplitude of transverse photovoltage is enabled by the broken symmetries of the electric and magnetic field patterns supported in the asymmetric triangle holes due to the interplay between the light helicity of circular polarization and the shape symmetries of triangle holes, together with the incident angle. These results will create opportunities for many applications relevant to nonlinear optics, photodetection, and chiral sensing.

Photo-induced dc voltage can be generated in various types of materials, such as semiconductor structures, topological insulators, quantum wells, and graphene, based on different physical origins including the photogalvanic effect,[1–6] electronic and plasmonic ratchet effect,[7–10] and photon drag effect.[11,12] The photon drag effect represents the generation of electrical current due to the momentum transfer from the absorbed photons to the free carriers in a conductive material. The photon drag effect can be described as one second-order nonlinear optical process, where the Lorentz force exerted on the conduction electrons in a conductor under optical excitation will form photo-induced voltage (PIV). The observed PIV perpendicular to the incident plane is referred to as transverse photo-induced voltage (TPIV). The photon drag effect induced PIV has been first studied in semiconductors such as germanium,[13,14] and it also exists on metal surfaces with or without surface plasmon resonance.[15–18] The photon drag effect in gold films enhanced by surface plasmon has been demonstrated with the PIV depending on the light incidence angle and polarization.[19] Photonic crystal and plasmonic structures can be utilized to further increase the PIV in semiconductors or metals.[20–24] TPIV signals from symmetric plasmonic structures such as gratings and circular holes have been observed with obliquely incident light induced broken symmetries.[22,23] It has been shown that the broken symmetry of the electric field in the plasmonic circular holes with obliquely incident light results in the TPIV generation and its sign change.[22–28] TPIV generated from the plasmonic nanovoids is due to the asymmetric field induced gradient force with obliquely incident light,[28] where the gradient force reverses for opposite circular polarization. Recently, TPIV has been calculated numerically in metal-dielectric-metal three-layer asymmetric plasmonic structures with normally incident light.[29]

In this work, two types of plasmonic symmetry-breaking isosceles-triangle holes and right-triangle holes in a single metal layer are designed to generate light helicity-dependent TPIV induced by the photon drag effect with normally and obliquely incident light. It is shown that the sign of TPIV reverses with the switched incident circular polarization for both types of plasmonic triangle holes. Furthermore, the unbalanced TPIV between two circular polarizations is achieved across the plasmonic right-triangle holes due to the higher degree of symmetry breaking, while the balanced TPIV is obtained for the plasmonic isosceles-triangle holes. The observed manipulation of the sign and the amplitude of TPIV originates from the asymmetric electric and magnetic field distributions in the symmetry-breaking triangle holes for right-handed and left-handed circularly polarized (RCP and LCP) light, as well as the difference of shape symmetries for isosceles-triangle holes and right-triangle holes. In addition, the amplitude variation of TPIV as a function of the light incident angle is also demonstrated. These results will open many opportunities for future applications in nonlinear optical devices, photodetectors, and optical sensors.

Figures 1(a) and 1(c) show the design for the two types of plasmonic triangle holes with different shape symmetries in a 50 nm-thick gold layer deposited on the glass substrate to generate TPIV. The first-type sample is the rectangle lattice of isosceles-triangle holes with a base of 190 nm, a height of 310 nm, and period dimensions of 410 nm by 310 nm along the *x* and *y* directions. The second-type sample is the right-triangle holes with a base of 200 nm, a height of 320 nm, and period dimensions of 430 nm by 310 nm. The isosceles-triangle hole possesses the mirror symmetry in the *x*-*z* plane, but the mirror symmetry of the *y*-*z* plane is broken; while the right-triangle hole further breaks the mirror symmetry in the *x*-*z* plane, it lacks any mirror symmetry. The shape symmetries of the triangle holes will affect the measured TPIV along the *y* direction across the plasmonic triangle hole arrays. The finite-integration time-domain (FITD) solver of the CST Studio Suite software is used to calculate the optical field distribution and the transmission, reflection, and absorption spectra from the plasmonic triangle hole. In the simulation, periodic boundary conditions are used along both *x* and *y* directions in the unit cell. The permittivity of glass is set as a constant of 2.25 and the permittivity of gold is obtained from the Drude model. Figures 1(b) and 1(d) display the simulated electric and magnetic field distributions on the *x*-*y* plane in the gold layer for the two types of asymmetric triangle holes under normally incident LCP and RCP light at the wavelength of 800 nm, which is close to the plasmonic resonance of the triangle holes. For the isosceles-triangle hole, the electric and magnetic fields show asymmetric patterns respect to the *x* axis with the field enhancement around the triangle corners, indicating that a net Lorentz force acted on electrons along the *y* direction and thus the TPIV signal. Furthermore, when the incident circular polarization is switched, the enhanced field hotspots are located in the mirror-symmetric locations in the triangle hole respect to the *x* axis, which will result in opposite Lorentz force and the reversed TPIV signal but with the unchanged amplitude. For the right-triangle hole with further broken shape mirror symmetry in the *x*-*z* plane, compared to the isosceles-triangle hole, the electric and magnetic field distributions under two circular polarizations will no longer be mirror-symmetric with respect to the *x* axis, so that the opposite Lorentz forces with unequal strengths, and therefore, the unbalanced TPIV signals are expected for normally incident LCP and RCP light.

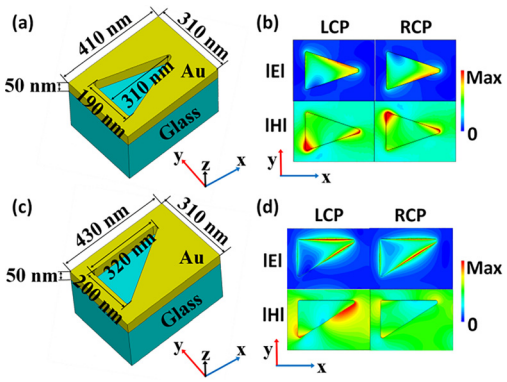

FIG. 1. (a) and (c) Schematics of the designed two types of plasmonic isosceles-triangle holes and right-triangle holes, respectively. (b) and (d) Simulated electric and magnetic field distributions on the *x*-*y* plane in the gold layer for the two types of triangle holes under normally incident LCP and RCP light at 800 nm.

For both types of plasmonic triangle holes, a single 50 nm-thick gold layer is deposited by electron beam evaporation on the glass substrate. Focused ion beam (FIB) milling (FEI Helios Nanolab 600, 30 kV, 9.7 pA) is utilized to fabricate the metasurface samples with an area of 50 μm by 50 μm. Figures 2(a) and 2(b) show the SEM images of the fabricated arrays of plasmonic isosceles-triangle holes and right-triangle holes, respectively. Figure 2(c) shows a SEM image of the sample area with cuts in the gold film which allow us to specify the two electrodes and measure the TPIV generated along the *y* direction. Figure 2(d) illustrates the schematic of the experimental setup to measure the TPIV. The incident beam with tunable wavelengths from 750 nm to 850 nm is generated from a femtosecond Ti:Sapphire laser (Coherent, Chameleon Ultra II, pulse width 140 fs, repetition rate 80 MHz) and then modulated at 153 Hz through an optical chopper. A linear polarizer and an achromatic quarter-wave plate are used to convert the incident light into a circularly polarized wave and switch the incident circular polarization. The incident laser beam is slightly focused on the metasurface sample by using a 4× objective lens with a laser spot size of around 50 μm. The generated electrical signal across the metasurface sample is then sent to a lock-in amplifier (Stanford Research Systems, SR830) for recording the TPIV by varying the optical power, wavelength, circular polarization, and beam incident angle.

The transmission and reflection spectra from the plasmonic triangle holes under circular polarization are measured using a collimated broadband Tungsten-Halogen white light source, where a linear polarizer and an achromatic quarter-wave plate are used to convert the incident light into a circularly polarized wave. The white light beam is focused normally onto the sample by a 50× objective lens, and the reflected light is collected by the same objective lens and coupled to a spectrometer (Horiba, iHR 550) through a beam splitter. The transmitted light is collected by another 10× objective lens to the spectrometer. Either a silver mirror or a transparent glass substrate is utilized to normalize the reflection or transmission spectra, respectively. Figure 3(a) plots the experimental and simulated transmission, reflection, and absorption spectra from the plasmonic isosceles-triangle holes under normally incident circularly polarized light. The spectra under LCP light will overlap with those under RCP light due

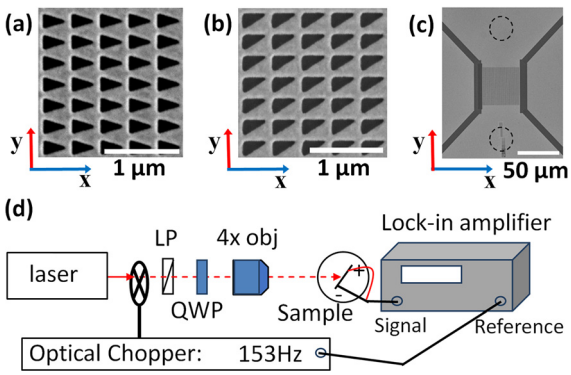

FIG. 2. (a) and (b) SEM images of the fabricated samples with isosceles-triangle holes and right-triangle holes, respectively. (c) SEM image of the sample with electrode cuts in the transverse configuration. Two dashed circles show the locations to connect two electrodes with thin gold wires. (d) Schematic of the experimental setup for recording the TPIV signal.

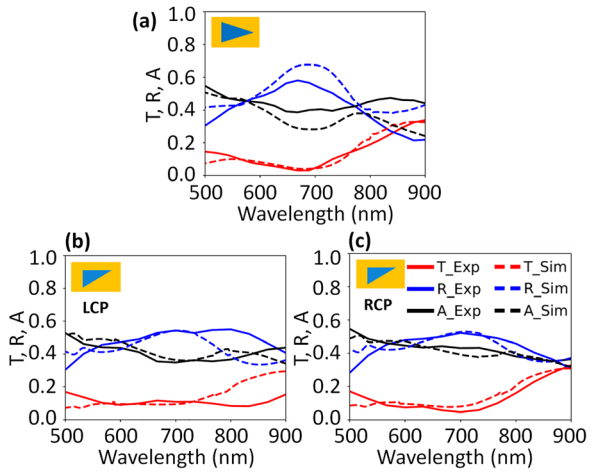

FIG. 3. (a) Experimental and simulated transmission (T), reflection (R), and absorption (A) spectra from the plasmonic isosceles-triangle holes under normally incident circularly polarized light. (b) and (c) Experimental and simulated T, R, and A spectra from the plasmonic right-triangle holes under normally incident circularly polarized light.

to the mirror symmetry in the *x-z* plane. The plasmonic resonance of the isosceles-triangle hole is located between 800 nm and 900 nm where the transmission is relatively high. In contrast, as shown in Figs. 3(b) and 3(c), the transmission, reflection, and absorption spectra from the plasmonic right-triangle holes exhibit different responses between normally incident RCP and LCP light, which is consistent with the simulated electric and magnetic field distributions for RCP and LCP light in Fig. 1(d) due to further broken shape mirror symmetry in the *x-z* plane for the right-triangle holes. The plasmonic resonance of the right-triangle hole is also designed between 800 nm and 900 nm, in order to compare the TPIV signals across the two types of plasmonic triangle holes.

As shown in Fig. 2(c), two electrodes perpendicular to the *x-z* plane are connected to collect the TPIV signal along the *y* direction across the plasmonic triangle hole array. The TPIV will be measured by changing the optical power, wavelength, and incident angle of the incident circularly polarized laser beam. Figure 4(a) shows the measured TPIV across the isosceles-triangle hole array as a function of optical power under normally incident RCP and LCP light at the wavelength of 800 nm, displaying the featured linear relation between

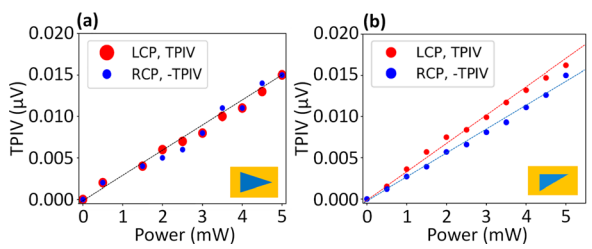

FIG. 4. (a) and (b) Linear dependence of the measured TPIV on the optical excitation power under normally incident RCP and LCP light at 800 nm for the plasmonic isosceles-triangle holes and right-triangle holes, respectively.

the photovoltage originated from the photon drag effect and optical excitation power for both circular polarizations. It is noted that the sign of TPIV flips, but the amplitude of TPIV remains almost unchanged when the circular polarization is changed due to the shape mirror symmetry in the *x-z* plane of the isosceles-triangle hole. The dashed line shows a linear fit to the measured TPIV, giving an external responsivity of around 2.8 nV/mW for both RCP and LCP incident light. With the focused laser spot size of around 50 μm on the sample, the corresponding responsivity is equivalent to 5.5 μV/(mW μm^{-2}). Figure 4(b) plots the optical power-dependent TPIV for the right-triangle hole array under normally incident RCP and LCP light. In contrast, the generated TPIV signal for LCP light is stronger than that for RCP light with the same optical excitation power, due to the further broken shape mirror symmetry in the *x-z* plane for the right-triangle hole. The external responsivity for RCP and LCP incident light is around 2.8 nV/mW and 3.2 nV/mW, respectively. Such an unbalanced TPIV signal under two circular polarizations can be explained from the mirror symmetry-breaking electric and magnetic field patterns with respect to the *x* axis as shown in Fig. 1(d).

The generated TPIV is measured for both types of plasmonic triangle holes with the optical power of 5 mW covering the wavelength range of 750 nm to 850 nm under normally incident RCP and LCP light, as shown in Fig. 5. For comparison, the TPIV with a negative sign for RCP light is plotted in order to illustrate the difference between the amplitude of TPIV for both circular polarizations. In both cases, the sign of TPIV flips as the incident circular polarization is switched, showing the helicity-dependent TPIV under normally incident light. For the isosceles-triangle holes, as shown in Fig. 5(a), the amplitude of TPIV at a specific wavelength is almost the same when the light helicity is changed from RCP to LCP. However, for the right-triangle holes, Fig. 5(b) shows the unbalanced TPIV with an obvious difference between the amplitude of TPIV generated under two circular polarizations in the whole wavelength range. The TPIV is also measured for both samples at an obliquely incident angle of $+15^{\circ}$ under RCP and LCP light with the optical power of 10 mW, as shown in Fig. 6. The behavior of the measured TPIV signal under obliquely incident light is quite similar to that for normally incident light, where the sign of TPIV depends on the incident circular polarization and either the balanced or unbalanced TPIV between two circular polarizations is achieved for the isosceles-triangle holes or the right-triangle holes.

The observed TPIV signal depending on light helicity and shape symmetries of triangle holes origins from the symmetry-breaking electric and magnetic field patterns supported in the triangle holes for

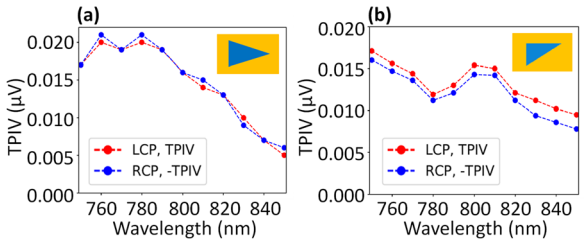

FIG. 5. (a) and (b) Measured TPIV for normally incident RCP and LCP light with the power of 5 mW in the wavelength range of 750–850 nm for the plasmonic isosceles-triangle holes and right-triangle holes, respectively. For better comparison, −TPIV for RCP light is plotted.

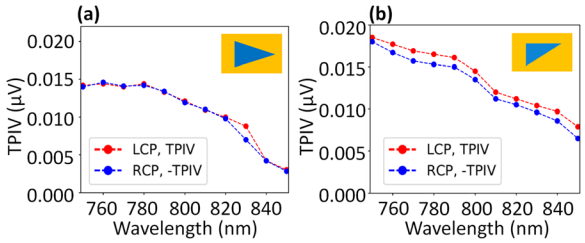

FIG. 6. (a) and (b) Measured TPIV at an obliquely incident angle of +15° under RCP and LCP light with the optical power of 10 mW in the wavelength range of 750–850 nm for the plasmonic isosceles-triangle holes and right-triangle holes, respectively.

RCP and LCP light. As illustrated in Figs. 1(b) and 1(d), for both types of asymmetric triangle holes, the field hotspots around the triangle sidewalls under two circular polarizations are shifted respect to the x axis when the circular polarization is changed, indicating the coupling between the spin angular momentum of photons and the orbital angular momentum of surface plasmons.[29,30] In particular, the isosceles-triangle hole possesses the mirror-reflected field profiles respect to the x axis under two circular polarizations so that the spin-to-angular momentum exchange is equivalent for RCP and LCP light and the balanced TPIV signal is obtained. However, the right-triangle hole supports the asymmetric shifts of field patterns respect to the x axis under two circular polarizations, which results in the unequal spin-to-angular momentum transfer and thus the unbalanced TPIV signal for RCP and LCP light. The origin of the generated TPIV from the asymmetric field patterns around the triangle holes can be further described by using the hydrodynamic model.[16,17]

Furthermore, the photon drag effect is proportional to the wave vector which is related to the photon momentum transfer to electrons. At oblique incidence, the photon drag induced current significantly changes due to the variation of the in-plane wave vector component. Figure 7 shows the measured TPIV as a function of the obliquely incident angle θ from −15° to +15° under RCP and LCP light with the optical power of 10 mW at 800 nm for the two types of plasmonic triangle holes. It is shown for both the metasurface samples that the measured TPIV signal is strongly dependent on the incident angle, which shows the unique feature of photon drag effect. For the isosceles-triangle holes, the TPIV amplitude decreases at large incident angle and reach the peak value at normal incidence, where the TPIV signal at normal incidence is around 1.5 times of that at the incident angle of +15°. By varying the incident angle, the in-plane component of the photon wave vector gets changed which results in the variation of the TPIV amplitude, manifesting the mechanism of photon drag effect instead of photogalvanic effect. It is well known that the TPIV has zero value for symmetric structures at normal incidence and TPIV signal shows an antisymmetric function of the incident angle.[20] In contrast, as plotted in Fig. 7(b), the TPIV from isosceles-triangle holes exhibits a maximum nonzero amplitude resulted from the large in-plane wave vector. Moreover, the TPIV has an asymmetric function of the incident angle, displaying the stronger TPIV at negative incident angles than those at positive incident angles, which is due to the interaction of asymmetric triangle holes and obliquely incident light. In addition, as shown in Fig. 7(d), the TPIV from right-triangle holes exhibits different responses, where the TPIV keeps increasing as the incident angle varies

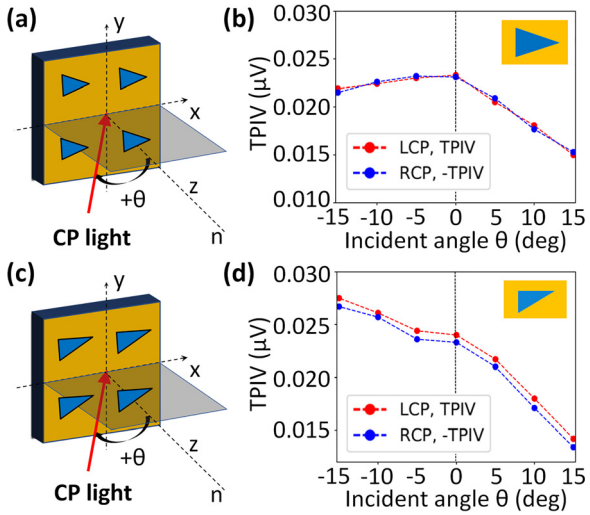

FIG. 7. (a) and (c) Illustration of the obliquely incident light with angle θ for the plasmonic isosceles-triangle holes and right-triangle holes, respectively. (b) and (d) The measured TPIV as a function of θ from −15° to +15° for RCP and LCP light with the optical power of 10 mW at 800 nm for the two types of triangle holes, respectively.

from +15° to −15° and the amplitude of TPIV for LCP light is always larger than that for RCP light at all incident angles, suggesting more symmetry-breaking effects from the right-triangle hole on the in-plane wave vector compared to the isosceles-triangle hole.

In summary, the plasmonic asymmetric isosceles-triangle holes and right-triangle holes have been designed to manipulate the generated transverse photo-induced voltage due to photon drag effect with normally and obliquely incident light. It is demonstrated that the sign of transverse photovoltage across the plasmonic triangle hole array depends on the incident light helicity and the amplitude difference of photovoltage between two circular polarizations is controlled by the shape symmetries of triangle holes. The observed response of the transverse photovoltage is explained by the symmetry-breaking analysis of the electromagnetic field distributions supported in both isosceles-triangle hole and right-triangle hole under circularly polarized incident light. The amplitude variation of TPIV depending on the incident angle is also demonstrated. These demonstrated results will open great possibilities for enabling future plasmonic and metasurface applications in nonlinear optics, polarization characterization, photodetection, and optical sensing.

The authors acknowledge support from the National Science Foundation under Grant No. ECCS-1653032 and DMR-1552871 and the Office of Naval Research under Grant No. N00014-16-1-2408. The authors thank the facility support from the Materials Research Center at Missouri S&T. The authors also thank Yuchao Zhang for the FIB milling of the gold film.

REFERENCES

[1]A. Lorke, S. Wimmer, B. Jager, J. P. Kotthaus, W. Wegscheider, and M. Bichler, Physica B **249–251**, 312 (1998).
[2]A. D. Chepelianskii, M. V. Entin, L. I. Magarill, and D. L. Shepelyansky, Eur. Phys. J. B **56**, 323 (2007).

[3]A. D. Chepelianskii, M. V. Entin, L. I. Magarill, and D. L. Shepelyansky, Physica E **40**, 1264 (2008).
[4]J. W. McIver, D. Hsieh, H. Steinberg, P. Jarillo-Herrero, and N. Gedik, Nat. Nanotechnnol. **7**, 96 (2012).
[5]P. Olbrich, L. E. Golub, T. Herrmann, S. N. Danilov, H. Plank, V. V. Bel'kov, G. Mussler, Ch. Weyrich, C. M. Schneider, J. Kampmeier, D. Grützmacher, L. Plucinski, M. Eschbach, and S. D. Ganichev, Phys. Rev. Lett. **113**, 096601 (2014).
[6]H. Plank, L. E. Golub, S. Bauer, V. V. Bel'kov, T. Herrmann, P. Olbrich, M. Eschbach, L. Plucinski, C. M. Schneider, J. Kampmeier, M. Lanius, G. Mussler, D. Grutzmacher, and S. D. Ganichev, Phys. Rev. B **93**, 125434 (2016).
[7]P. Olbrich, E. L. Ivchenko, R. Ravash, T. Feil, S. D. Danilov, J. Allerdings, D. Weiss, D. Schuh, W. Wegscheider, and S. D. Ganichev, Phys. Rev. Lett. **103**, 090603 (2009).
[8]P. Olbrich, J. Kamann, M. Konig, J. Munzert, L. Tutsch, J. Eroms, D. Weiss, M.-H. Liu, L. E. Golub, E. L. Ivchenko, V. V. Popov, D. V. Fateev, K. V. Mashinsky, F. Fromm, Th. Seyller, and S. D. Ganichev, Phys. Rev. B **93**, 075422 (2016).
[9]V. V. Popov, D. V. Fateev, T. Otsuji, Y. M. Meziani, D. Coquillat, and W. Knap, Appl. Phys. Lett. **99**, 243504 (2011).
[10]I. V. Rozhansky, V. Yu. Kachorovskii, and M. S. Shur, Phys. Rev. Lett. **114**, 246601 (2015).
[11]H. Diehl, V. A. Shalygin, V. V. Bel'kov, Ch. Hoffmann, S. N. Danilov, T. Herrle, S. A. Tarasenko, D. Schuh, Ch. Gerl, W. Wegscheider, W. Prettl, and S. D. Ganichev, New J. Phys. **9**, 349 (2007).
[12]J. J. Karch, P. Olbrich, M. Schmalzbauer, C. Zoth, C. Brinsteiner, M. Fehrenbacher, U. Wurstbauer, M. M. Glazov, S. A. Tarasenko, E. L. Ivchenko, D. Weiss, J. Eroms, R. Yakimova, S. Lara-Avila, S. Kubatkin, and S. D. Ganichev, Phys. Rev. Lett. **97**, 227402 (2010).
[13]A. M. Danishevskii, A. A. Kastal'skii, S. M. Ryvkin, and I. D. Yaroshetskii, Sov. Phys. JETP **31**, 292–295 (1970).
[14]A. F. Gibson, M. F. Kimmitt, and A. C. Walker, Appl. Phys. Lett. **17**, 75–77 (1970).
[15]J. E. Goff and W. L. Schaich, Phys. Rev. B **61**, 10471 (2000).
[16]J. E. Goff and W. L. Schaich, Phys. Rev. B **56**, 15421–15430 (1997).
[17]H. Kurosawa, S. Ohno, and K. Nakayama, Phys. Rev. A **95**, 033844 (2017).
[18]M. Akbari, J. Gao, and X. Yang, Opt. Express **26**, 21194–21203 (2018).
[19]A. S. Vengurlekar and T. Ishihara, Appl. Phys. Lett. **87**, 091118 (2005).
[20]T. Hatano, B. Nishikawa, M. Iwanaga, and T. Ishihara, Opt. Express **16**, 8236–8241 (2008).
[21]I. Ishihara, Phys. Status Solidi A **201**, 398–404 (2004).
[22]T. Hatano, T. Ishihara, S. G. Tikhodeev, and N. A. Gippius, Phys. Rev. Lett. **103**, 103906 (2009).
[23]H. Kurosawa and T. Ishihara, Opt. Express **20**, 1561–1574 (2012).
[24]N. Noginova, V. Rono, F. J. Bezares, and J. D. Caldwell, New J. Phys. **15**, 113061 (2013).
[25]M. M. Glazov and S. D. Ganichev, Phys. Rep. **535**, 101–138 (2014).
[26]M. Akbari, M. Onoda, and T. Ishihara, Opt. Express **23**, 823–832 (2015).
[27]M. Akbari and T. Ishihara, Opt. Express **25**, 2143–2152 (2017).
[28]N. V. Proscia, M. Moocarme, R. Chang, I. Kretzschmar, V. M. Menon, and L. T. Vuong, Opt. Express **24**, 10402–10411 (2016).
[29]Q. Bai, Opt. Express **23**, 5348–5356 (2015).
[30]Y. Gorodetski, N. Shitrit, I. Bretner, V. Kleiner, and E. Hasman, Nano Lett. **9**, 3016–3019 (2009).